Presented at the IEEE Pulsed Power & Plasma Science Conf., San Francisco, CA, June 2013

SAND2013-nnnn

SAND2013-4936C

DESIGN AND OPTIMIZATION OF MAGNETICALLY-APPLIED PRESSURE-SHEAR (MAPS) EXPERIMENTS ON SANDIA'S Z MACHINE

Thomas A. Haill[1], C. Scott Alexander, Devon G. Dalton, Dean C. Rovang and Derek C. Lamppa

Pulse Power Sciences Center, Sandia National Laboratories[2]

PO Box 5800, Albuquerque, NM, 87185-1189, USA

Abstract

Magnetically-applied pressure-shear (MAPS) is a recently developed technique to directly measure material shear strength using magnetohydrodynamic (MHD) pulsed power platforms [1,2]. The method has been prototyped on Sandia's Veloce pulser, but was limited to strength measurements at modest pressures of ~10 GPa. Our present aim is to develop MAPS into a robust technique to measure strength at higher pressures achievable on Sandia's Z pulsed power machine.

I. INTRODUCTION TO THE MAPS CONCEPT

By applying an external static magnetic field longitudinally to a tri-layer driver/sample/anvil region, the MHD drive in the driver layer directly induces a shear stress wave in addition to the usual longitudinal stress wave. The two stress waves propagate at their respective wave speeds into the sample and anvil layers. In the sample layer, the longitudinal and shear deviatoric stresses are coupled and limited by a von Mises yield criterion; hence the transmissible shear wave at a given pressure is limited by the sample material strength. In the anvil layer, the transmitted pressure and shear are directly related to the measured free surface velocities of the anvil which are measured using a transverse VISAR diagnostic.

Complex wave interactions among forward and reflected longitudinal and shear waves, the advancing magnetic diffusion front of the MHD drive, the shape of the current drive, as well as the applied magnetic field strength and uniformity, makes the design of the experiments complex. The MAPS experiments are modeled using Sandia's ALEGRA MHD code.

The MAPS method directly measures strength a high pressures. Other techniques that directly measure strength, such as Hopkison bar, oblique impact and lateral gauges, are limited to lower pressures. Indirect measurement techniques, such as wave profile analysis and stress difference analysis, require various assumptions in order to carry out the analysis or may be prone to large uncertainties. Still other methods, such as Rayleigh-Taylor perturbation growth, require accurate well-parameterized strength models which are unknown and for which the parameters are being measured.

This paper presents the design and optimization of MAPS experiments to be fielded on Z. Section II presents the basic MAPS coaxial load design which is based upon a history of coaxial loads and quasi-isentropic compression experiments previously fielded on Z, and also describes the applied magnetic field coil design necessary to induce shear in the load. Section III overviews the physics and the numerical 2D MHD investigations that optimize MHD shear generation, longitudinal and shear wave coupling, and timing of the wave interactions. The optimized MHD current profile is reproduced by a Z machine circuit model ready for carrying out the experiments. Finally in Section IV we summarize our findings.

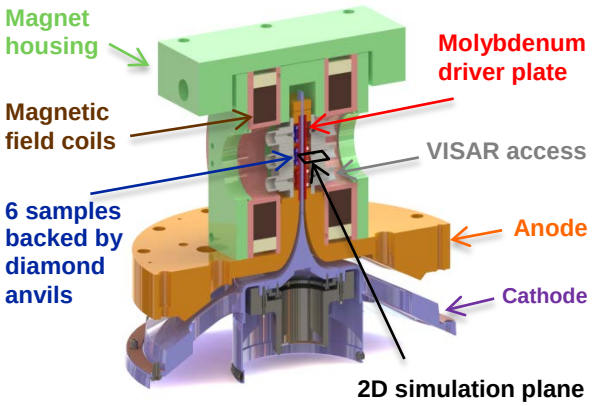

Figure 1. Notional diagram of the MAPS load on the Z machine. A 2D simulation plane is located at the center sample of the coaxial load. The longitudinal direction is through the thickness of the panel (x) and the shear direction is across the width of the panel (y). Current flows along the height of the panel (z).

[1] Electronic address: tahaill@sandia.gov

[2] Sandia National Laboratories is a multi-program laboratory managed and operated by Sandia Corporation, a wholly owned subsidiary of Lockheed Martin Company, for the U. S. Department of Energy's National Nuclear Security Administration under contract DE-AC04-94AL85000.

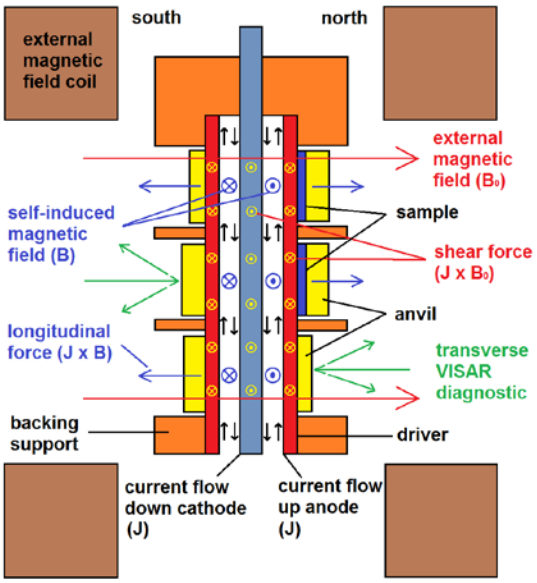

Figure 2. Vertical cross-sectional view along the height and longitudinally through the coaxial load outlining the key features of the MAPS experimental technique on the Z machine. See text for details.

II. DESIGN OF MAPS FOR Z

A. Z Coaxial Load Design

MAPS on Z utilizes a well-tested coaxial load design used for isentropic compression and high-velocity flyer experiments [3,4,5,6]. Figure 1 shows a notional 3D diagram of the MAPS coaxial design with the addition of applied magnetic field coils and associated housing. The diagram has been cut on a vertical plane and longitudinally through the load and labeling major components.

Figure 2 shows a vertical cross-section along the height and longitudinally through the coaxial load and outlines the key features of the MAPS concept. The pulsed power drive generates a current (J) that initially flows upward along the 28×5.5-mm interior surface of anode and downward along the 14×2 mm cathode. The current induces a nearly spatially uniform magnetic field (B) in the 1.75 mm gaps between the anode and cathode. The magnetic field depends on the anode separation D and cathode width W according to:

$$B(t) = \frac{\mu_0 I(t)}{L(t)} = \frac{\mu_0 I(t)}{2\left[D(t) + W(t)\right]} \qquad (1)$$

The time dependence of the length scale is affected by geometry deformation and magnetic field diffusion through the electrodes, but to first order L=39 mm. For peak currents in the range 8.5 to 11 MA, the peak magnetic field in the gap is between ~275 to 355 T, with a corresponding magnetic field pressure of ~30 to 50 GPa.

The Lorentz interaction with the self-consistent magnetic field $J \times B$ accelerates the anode panels away from each other and produces a longitudinal pressure wave which compresses the sample material to pressures on the order of 30 to 50 GPa. This describes the behavior of standard Z coaxial loads. For MAPS, a long-pulse 7-10 T external magnetic field (B_o) is applied to the load region using external coils. The Lorentz interaction with the applied field $J \times B_o$ produces a shear wave in the driver layer of the composite panel which then propagates through the sample material where it is truncated to a level determined by the sample strength.

The tri-layer anode panel is comprised of driver, sample, and anvil layers. The driver must have suitably high electrical conductivity to allow for an MHD drive and to inhibit magnetic field diffusion. The driver must also have greater strength than the sample material and the shear wave generated in the driver must be of sufficient magnitude in order for the shear in the sample to reach the yield surface of the sample.

The sample layer is backed by an anvil that is also stronger than the sample, and preferably remains elastic. If the anvil is elastic, then it will support the entire shear passed by the sample layer and there will be no attenuation of the transmitted shear waves and an accurate measurement of the sample strength can be made.

Finally, specialized VISAR interferometry is used to record both longitudinal and transverse particle velocities at the free surface. Pressure and strength are calculated from the measured particle velocities.

The materials selected for the three panel layers in the first set of MAPS experiments on Z are a molybdenum driver layer, a tantalum sample layer, and a diamond anvil. Some properties of these materials are listed in Table 1.

The load design shown in Figure 2 accommodates 6 experiments grouped into 3 pairs. The middle pair of experiments on the centerline of the applied magnetic field coils is the primary MAPS experiment. The middle right panel has a tantalum sample, whereas the middle left panel omits the sample. The left experiment with no sample measures shear generation in the drive layer and verifies truncation of the shear as it passes through the sample layer on the opposing right side. The top pair of experiments are similar to the middle pair, but are located off of the coil symmetry axis in a region where the applied magnetic field is expected to be more non-uniform. The effect of magnetic field gradients will be determined by this experiment. Finally, the bottom pair of experiments is designed to measure the longitudinal and shear wave speeds of the diamond anvils used in these experiments.

Table 1. MAPS Materials and Simulation Model Parameters

Panel Layer Material	Equation of State	Strength Model	Conductivity Model	Density (g/cm^3)	Longitudinal Wave Speed (km/s)	Shear Wave Speed (km/s)	Yield Strength (GPa)
Driver Molybdenum	LANL Sesame 2984	CTH Elastic Plastic w/ Steinberg-Guinan-Lund	Lee-More-Desjarlais (LMD)	10.22	6.45-6.45 [16,17]	3.47-3.48 [16,17]	0.9
Sample Tantalum	LANL Sesame 3720	CTH Elastic Plastic w/ Steinberg-Guinan-Lund	Lee-More-Desjarlais (LMD)	16.654	3.35-4.16 [16]	2.07-2.09 [16,17]	0.375
Anvil Dimond	LANL Sesame 7834	CTH Elastic Perfectly Plastic	Insulator	3.5126	18.328 [18,19]	11.659-12.0 [18,19]	50-90

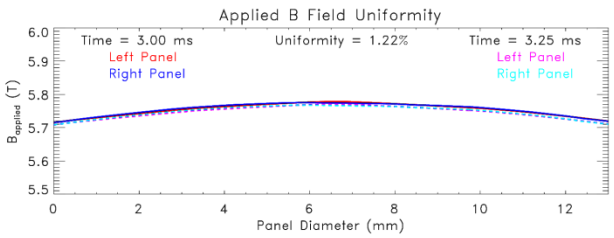

Figure 3. Long-pulse applied field coils produce a temporally and spatially uniform magnetic field at the central sample region.

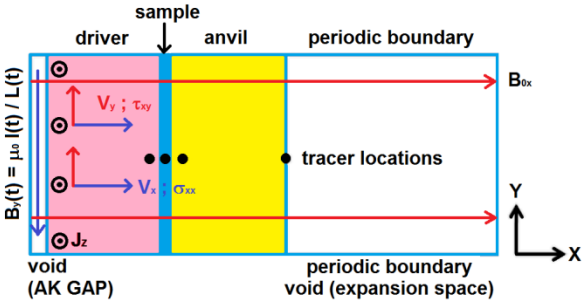

Figure 4. Illustration of the 2D computational domain used for high resolution MAPS simulations. Variables are a function of the x coordinate only. Transverse motion and shear is allowed. The simulation domain is periodic in the y direction.

B. Applied Magnetic Field Coil Design

The capability to apply uniform external magnetic fields is of interest to several areas of research on the Z pulsed power facility [7]. Besides these MAPS experiments which are part of the Dynamic Materials Properties (DMP) program, Sandia's Inertial Confinement Fusion Program (ICF) is evaluating the modification of fusion plasma particle transport properties via flux compression of applied magnetic fields to >50 MGauss in the Magnetized Liner Inertial Fusion (MagLIF) concept [8]. The magnetic field generation requirements for the different research areas are similar and have overlapping requirements for field strength (1–10 T), pulse length (1–10 ms), magnet size (bore diameter and length ~ 1–10 cm), magnetic field energy (10 – 100 kJ) and split-magnet topologies for diagnostic and sample access.

The applied magnetic field coils are developed and tested at the System Integration Test Facility (SITF). According to design simulations, the long-pulse ~4.75 ms FWHM current pulse will drive a temporally and spatially uniform magnetic field for these MAPS experiments. Figure 3 shows that the applied field is uniform to 1.2% across the middle pair of samples. There is very good uniformity between the left and right panels. Also, there is <0.5% temporal uniformity for at least 0.25 ms near the peak of the current pulse. Note the 3 order-of-magnitude difference in time scales between the applied field current pulse (ms) and the duration of the MAPS experiment (μs).

III. OPTIMIZATION OF MAPS FOR Z

As with any set of experiments, a firm understanding of the physics is necessary to design, optimize and analyze the experiments. The best understanding is often achieved through simplified models augmented by computer simulation. The MAPS experiments are modeled using Sandia's ALEGRA-MHD simulation code [9,10]. ALEGRA-MHD is an operator-split, multi-physics, multi-material, arbitrary Lagrangian-Eulerian code developed to model isentropic compression experiments (ICE), stripline flyer plate assemblies, wire-array and gas puff Z pinch implosions, ceramic fracture, and electromagnetic launch.

Figure 4 illustrates the computational domain used for the MAPS simulations. We assume that all variables are a function of the x coordinate only and time t, that the non-zero velocity components are (V_x, V_y), that the non-zero magnetic field components are (B_{0x}, B_y), and that the only non-zero component of the current density J_z is orthogonal to the mesh. The externally applied longitudinal magnetic field B_{0x} is constant in space and time.

The initial conditions are that the velocity and the self-consistent transverse magnetic field B_y are zero. A tangent magnetic field boundary condition of the form given by Equation 1 is applied in the AK gap at the left-hand boundary of the mesh. B_y is zero at the right-hand boundary. Periodic boundary conditions are applied at the top and bottom boundaries of the simulation domain, thus material that flows off the top of the mesh re-enters at the bottom of the mesh.

Lagrangian tracer points that move with the material are located horizontally throughout the driver, sample and anvil layers to query the state of the materials and the propagation of longitudinal and shear waves. The four most significant tracers are noted in Figure 4. Table 1 lists the material models utilized in these simulations.

The Z load current pulse is parameterized to facilitate optimization of the MAPS experiments according to Equation 2.

$$I(t) = I_{peak} \bullet \begin{cases} \left[\frac{1-\cos\left(\pi \cdot t / t_{peak}\right)}{2}\right]^{p} & ;t \le t_{peak} \\ \left[\frac{1+\cos\left(\pi \cdot \left(t - t_{peak}\right) / t_{fall}\right)}{2}\right]^{q} & ;t \ge t_{peak} \end{cases} \quad (2)$$

I_{peak} is the peak of the load current. Asymmetric pulses have separate times for the rise to peak current t_{peak} and the fall from peak current after the peak t_{fall}. The shape of the rise and fall are controlled by the exponents p and q. Lower values of p and q represent broader FWHM pulses, whereas higher values represent narrower FWHM pulses.

A. Physics of the Driver Layer

The purpose of the driver layer is to generate both the longitudinal and shear waves that are passed into the sample. The molybdenum driver layer is modeled using a Sesame tabular equation of state [11], the Steinberg-Guinan-Lund elastic-plastic strength model [12], and the Lee-More-Desjarlais electrical and thermal conductivity model [13].

A critical aspect of MAPS is that both the longitudinal and the shear waves must propagate faster than and separate from the magnetic diffusion front in the driver. An accurate conductivity model is paramount for modeling the magnetic field diffusion rate. To assess the accuracy of LMD molybdenum electrical conductivity model we compare ALEGRA-MHD to published data in Figures 5 [14,15]. Below melt ALEGRA-MHD agrees very well with published data. As the molybdenum changes state from solid to liquid there is a corresponding jump (drop) in resitivity (conductivity). The published data indicate that liquid molybdenum in ALEGRA-MHD is slightly too resistive. This will tend to over-predict the partitioning of current in solid molybdenum and under-predict the current in the melted molybdenum, as well as over-predict the Joule heating of the liquid molybdenum and the heat transfer to the solid molybdenum. The end result is that these simulations represent a worst case, conservative estimate of the magnetic diffusion through the drive layer at rates of 1 to 1.5 km/s.

Accurate longitudinal and shear wave speeds are also important to the timing of forward and reflected waves. Figure 6 shows the longitudinal and shear waves speeds for both molybdenum and diamond as a function of pressure along the material isentropes and the agreement with published data at ambient conditions [16,17,18,19].

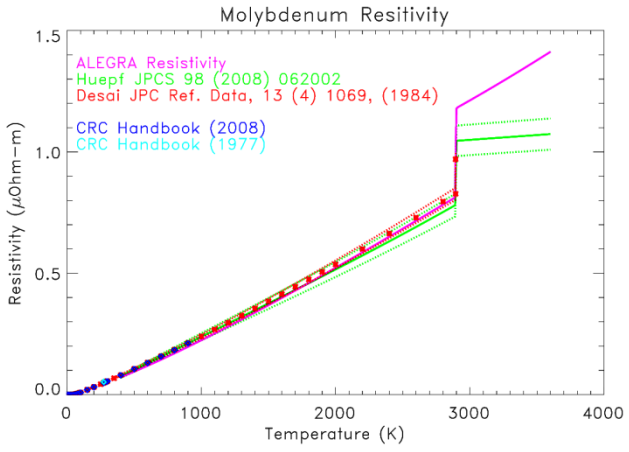

Figure 5. Comparison of the molybdenum LMD conductivity model to published data as a function of temperature up to melt.

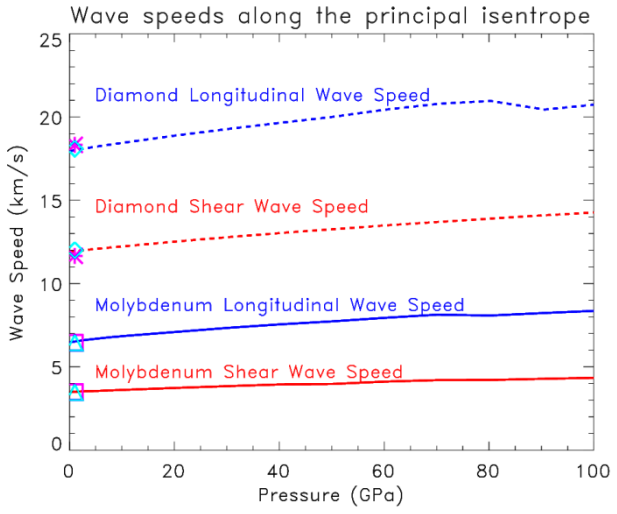

Figure 6. Plot of molybdenum and diamond wave speed along the principal isentrope of each material from 0 to 100 GPa as determined by ALEGRA.

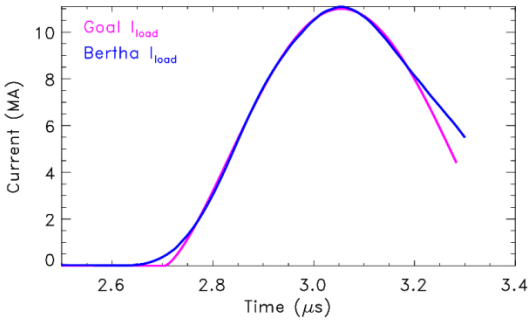

Figure 7. Comparison of the goal load current profile designed through optimization of MHD simulations and the predicted Z machine load current profile designed to match the goal current.

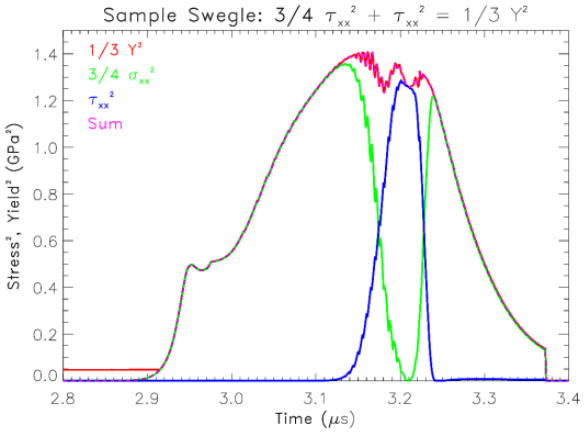

Figure 8. Components of the von Mises yield criterion for the predicted MAPS experiment on Z.

B. Physics of the Sample Layer

The success of MAPS relies upon the constraint imposed by the von Mises relation between the deviatoric stresses and the yield stress [20]. The von Mises yield criterion is:

$$\sum_j \sum_i \tau_{ij} \cdot \tau_{ij} \le \frac{2}{3}\left(Y(P)\right)^2 \tag{3}$$

The right-hand side yield stress $Y(P)$ is a function of the hydrostatic pressure which is the first invariant of the total material stress. The left-hand side is the second invariant of the deviatoric stress tensor τ_{ij}. The deviatoric stress is symmetric, $\tau_{ij} = \tau_{ji}$, and traceless, $\tau_{yy} = \tau_{zz} = -1/2 \cdot \tau_{xx}$. The design of MAPS also imposes $\tau_{xz} = \tau_{yz} = 0$. Therefore Equation 3 reduces to:

$$\frac{3}{4}\tau_{xx}^2 + \tau_{xy}^2 \le \frac{1}{3}Y^2 \tag{4}$$

This is a useful form of the von Mises yield criterion derived by Swegle and Chhabildas [21]. A plot of this criterion is shown in Figure 8 for the predicted MAPS experiment. A discussion of this relation can be found in Section D.

C. Physics of the Anvil Layer

MAPS utilizes elastic anvils. Linear elastic theory relates the longitudinal σ_{xx} and shear τ_{xy} stresses at the drive surface of the anvil to the longitudinal $u_{fs}^{long.}$ and transverse $u_{fs}^{trans.}$ velocities [22,23]. The theory provides a direct measure of the longitudinal and shear stresses in the sample according to Equations 5 and 6.

$$\sigma_{xx} = \rho_0 C_L u_p^{long.} = \frac{1}{2}\rho_0 C_L u_{fs}^{long.} \tag{5}$$

$$\tau_{xy} = \rho_0 C_S u_p^{trans.} = \frac{1}{2}\rho_0 C_S u_{fs}^{trans.} \tag{6}$$

D. Results of Optimization and Prediction of Experimental Results

Optimization of the MAPS experiment is accomplished by systematic parameter variation, including panel layer thicknesses, applied magnetic field strength, and load current profile. However, the load current and pulse shape provides the greatest flexibility in optimizing the MAPS experiments

Shear waves travel slower than longitudinal waves. If the molybdenum driver layer is too thick then the shear wave arrives in the sample too late. If the drive layer is too thin, then the magnetic field can diffuse through into the sample. A drive layer thickness of 1 mm is good compromise between these competing effects.

The tantalum sample layer is driven to yield therefore longitudinal and shear waves will attenuate. A sample thickness of 0.1 mm limits the attenuation, yet is a good thickness for manufacturability.

The diamond anvil thickness must be large enough that longitudinal release waves returning from the free surface back to the sample do not compromise the forward shear waves arriving from the driver. The 18 km/s longitudinal wave speed in diamond implies a 0.22 µs round trip transit time in a 2 mm thick anvil. While it is desirable to lengthen this time, this anvil thickness is the largest thickness readily available.

The peak current is determined by the peak pressure desired in the sample layer. As noted previously, peak currents of 8.5 and 11 MA produce corresponding pressures of 30 and 50 GPa, respectively.

The minimum applied magnetic field strength is constrained by need for the shear stress wave to be able to

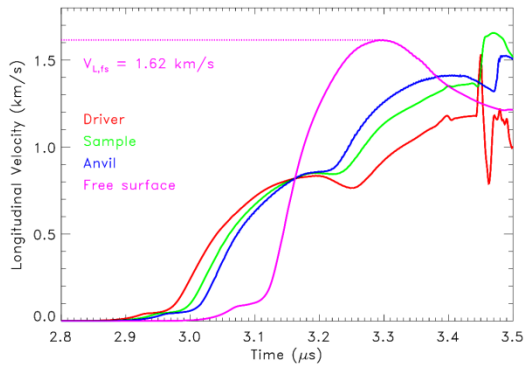

Figure 9. Simulated longitudinal velocities near the sample layer and at the anvil free surface. The anvil free surface velocity is a prediction of the VISAR experimental velocity expected on Z.

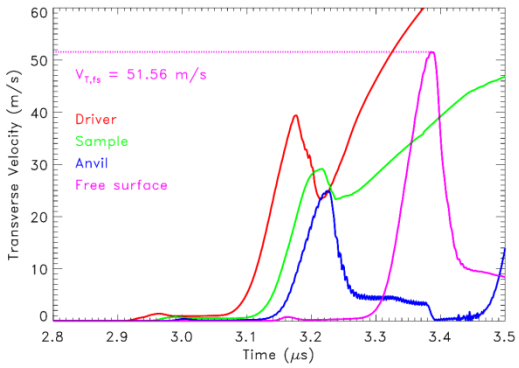

Figure 10. Simulated and unfolded transverse stress near the sample layer and at the anvil free surface. The anvil free surface velocity is a prediction of the VISAR experimental velocity expected on Z.

drive the sample to the maximum yield stress that the sample can support. No significant difference is seen in simulations run at 7 and 8 T applied field magnitudes, therefore we choose an applied field value of 8 T. Because the longitudinal and shear stress waves are not directly coupled, the shear wave timing is independent of the applied magnetic field.

The shape of the current pulse provides the greatest tool for optimizing the MAPS experiments. If the current rise time is too long, then the shear wave arrives too late because the pressure in the sample releases too soon due to the release waves returning from the free surface. If the current rise time is too short, then the magnetic field can diffuse through the molybdenum driver before the shear wave can separate from the magnetic diffusion front. Also, fast rise current pulses may produce shocks in driver rather than ramp compression waves. The final constraint is that the optimized current pulse be realizable on the Z machine.

Figure 7 shows the idealized load current profile designed though the optimization process. This current pulse produces 50 GPa pressure in the sample and has the peak shear stress wave arrive near the maximum of the pressure pulse. The idealized current profile is converted into a Z machine load current profile. The Z machine has 36 independently programmable pulse forming lines that allow a practically unlimited number of current waveforms. Bertha is a design tool that models the Marx generators pulse forming sections, vacuum transmission lines, and load and is used to determine the Z machine settings necessary to produce the desired current profile [24]. Figure 8 overlays the Bertha computed load current with the idealized MAPS current showing that the goal current is achievable on the Z machine.

Results of the ALEGRA-MHD simulation of the MAPS load driven by the Bertha load current are shown in Figures 8 to 12.

Figure 8 shows the von Mises yield criterion and deviatoric stress wave timing in the tantalum sample. Between about 2.9 and 3.1 μs the longitudinal stress wave compresses the sample layer. The yield stress $Y(P)$ increases as a function of increasing pressure (as well as strain, strain-rate, temperature, etc.). During compression there is a substantial longitudinal deviatoric stress component τ_{xx} that is limited by the yield stress. Near peak pressure between about 3.1 and 3.25 μs, the sample is in transition from being compressed to becoming released. During this interval the on-diagonal deviatoric stress components τ_{xx}, τ_{yy} and τ_{zz} decrease in amplitude, pass through zero and change sign. This occurs independent of the presence of the shear stress τ_{xy}, thus the drop of τ_{xx}^2 to zero always happens and the von Mises criterion is an inequality if no shear is present.

With the presence of the applied field a shear stress wave τ_{xy} is generated. This wave is timed so that the peak of the shear stress arrives when the longitudinal deviatoric stress is zero at about 3.2 μs. If the shear stress wave is strong enough, then the state of the sample material is driven to the yield surface, re-establishing the equality of the von Mises criterion. If such is the case, then the yield stress may be computed as:

$$Y = \sqrt{3} \cdot \tau_{xy} \tag{7}$$

Note that if the shear stress wave arrives early or late relative to the minimum in the longitudinal deviatoric stress, then a shear wave is transmitted that is less than yield stress and Equation 7 would not hold. In this simulation the shear wave pulse is narrower than longitudinal wave dip, therefore minor dips are seen in Y^2 as computed by the strain-rate-dependent Steinberg-Guinan-Lund strength model. No such dips are seen if the strain-rate-independent Steinberg-Guinan model is used.

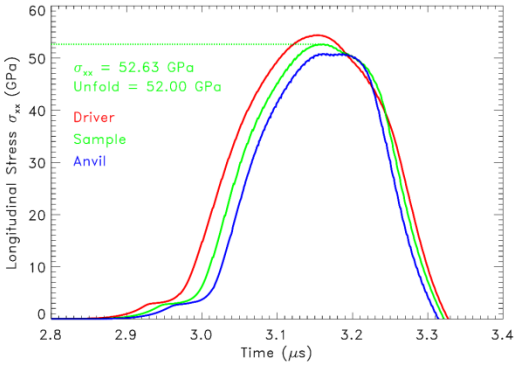

Figure 11. Simulated and unfolded longitudinal stress near the sample layer. The stress unfolded from the free surface longitudinal velocity compares favorably to the simulated peak stress.

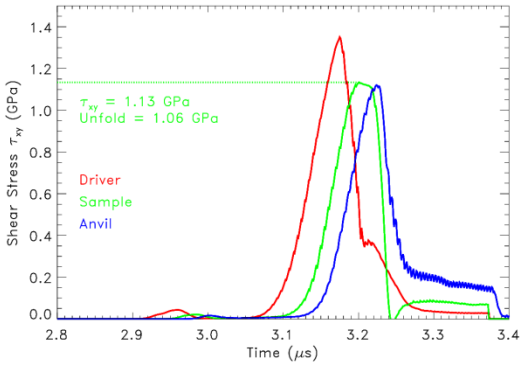

Figure 12. Simulated and unfolded shear stress near the sample layer. The shear stress unfolded from the free surface transverse velocity compares favorably to the simulated peak stress.

Finally, the effect of the reflected longitudinal wave from the free surface of the diamond anvil is seen in Figures 8 and 11. Between about 3.15 and 3.23 μs there is a slight asymmetry in the peak pressure and in Y^2. This occurs 2.2 μs after the initial arrival of the pressure pulse at 2.9 μs, and signals the return of the elastic precursor after the 2.2 μs roundtrip transit time from the sample through the anvil to the free surface and back. If the thickness of the diamond anvil could be increased, this would also increase the transit time and mitigate this slight asymmetry in pressure and yield.

Figures 9 and 10 plot the longitudinal and transverse velocities in the driver just before the sample, in the sample, in the anvil just after the sample, and at the anvil free surface, respectively. Clearly seen in these plots is the velocity doubling at the free surface. In Figure 10, the first peak of the transvers velocity coincides with the peak of the shear stress. The secondary rise in the longitudinal and transverse velocity, coupled with the low transverse velocity in the anvil after ~2.27 μs, signals the arrival of the magnetic diffusion front. The material cannot support shear due to the von Mises coupling. Late time features in the longitudinal velocity and the drop of the transverse velocity to near zero after about 3.4 μs signal the arrival of the melt wave in the sample.

Figures 11 and 12 plot the longitudinal and transverse stresses in the driver just before the sample, in the sample, and in the anvil just after the sample, respectively. By querying the simulation stresses near the sample, we can show the consistency of using linear elastic theory for anvil. Substituting the anvil density and longitudinal and shear wave speeds, as well as the peaks of the simulated longitudinal and transvers free surface velocities into Equations 12 and 13, the peak sample longitudinal and shear stresses are computed to be 52.0 and 1.06 GPa, respectively. These compare directly to the simulated peak sample longitudinal and shear stresses of 52.63 and 1.13 GPa, and agree to 1.2% and 6.2%, respectively.

IV. CONCLUSIONS

MAPS is a novel technique that directly measures material strength at high pressures. This investigation achieves the goal of porting the MAPS method to Sandia's Z machine. We designed a coaxial Z load that provides a nearly constant applied magnetic field across a 13 mm diameter tri-layer panel. Through extensive use of MHD simulation, pressure and shear waves in a tri-layer molybdenum / tantalum / diamond (driver/sample/anvil) panel were timed so that the peak of the shear stress wave coincides closely with peak in the total longitudinal stress (pressure) wave and also a minimum in the longitudinal deviatoric stress wave, thereby satisfying a particular form of the von Mises yield criterion. We described how pressure and yield stress may be directly computed from the longitudinal and transverse particle speeds measured at the anvil free surface using a transverse VISAR diagnostic. An idealized load current drive was designed and optimized, and a Z machine configuration was developed that produces this idealized load current. This machine configuration was used to predict Z-MAPS experiments. MAPS experiments on Z are scheduled.

The authors wish to thank R. Lemke, J.-P. Davis, and J. Brown for their tutelage in the use of Bertha to design Z current profiles. We acknowledge M. Desjarlais and M. French for discussions regarding molybdenum electrical conductivity. Finally, we acknowledge J. Asay and J. Ding for helpful technical discussion regarding strength of materials.

V. REFERENCES

[1] C.S. Alexander, J.R. Asay, and T.A. Haill, "Magnetically applied pressure-shear: A new method for direct measurement of strength at high pressure," J. Appl. Phys., **108**, 126101 (2010).

[2] T.A. Haill, C.S. Alexander, and J.R. Asay, "Simulation and analysis of magnetically applied pressure-shear (MAPS) experiments," Digest of Technical Papers, 2011 IEEE Pulsed Power Conference, R.D. Curry and B.V. Oliver, eds., pp. 1093 (2011).

[3] C. A. Hall, *et al*., "Experimental configuration for isentropic compression of solids using pulsed magnetic loading," Rev. Sci. Instrum., 72 (9) 3587 (2001).

[4] J.-P. Davis, et al., "Magnetically driven isentropic compression to multimegabar pressures using shaped current pulses on the Z accelerator," Phys. Plasmas, **12**, 056310 (2005).

[5] R.W. Lemke, *et al*., "Self-consistent, two-dimensional, magnetohydrodynamic simulations of magnetically driven flyer plates," Phys. Plasmas, **10** (5) 1867 (2003).

[6] R.W. Lemke, *et al*., "Magnetically accelerated, ultrahigh velocity flyer plates for shock wave experiments," J. Appl. Phys., **98**, 073520 (2005).

[7] D.C. Rovang, D.C. Lamppa, A.C. Owen, *et al*., "Status of the applied magnetic field capability on Z," IEEE Pulsed Power Plasma Science Conference, San Francisco, CA (2013).

[8] S.A. Slutz et al., "Pulsed-power-driven cylindrical liner implosions of laser preheated fuel magnetized with an axial field", Phys. Plasmas, **17,** 056303 (2010).

[9] A.C. Robinson, et al., "ALEGRA: An Arbitrary Lagrangian-Eulerian Multimaterial, Multiphysics Code," AIAA 2008-1235, 46th AIAA Aerospace Science Meeting and Exhibit, Reno, NV (2008).

[10] A.C. Robinson, J.H.J. Niederhaus, and E. Love, "Arbitrary Lagrangian-Eulerian 3D ideal MHD algorithms," Int. J. Numer. Meth. Fluids, **65**, 1438 (2010).

[11] K.S. Holian, ed., "Handbook of Material Property Data Bases, Vol. 1c: Equations of State" Tech. Report LA-10160-MS, Los Alamos National Laboratory, Nov. 1984.

[12] D.J. Steinberg, S.G. Cochrane, and M.W. Guinan, "A constitutive model for metals applicable at high strain rate," J. Appl. Phys., **51** (3) 1498 (1980); D.J. Steinberg and C.M. Lund, "A constitutive model for strain rates from 10^{-4} to 10^{6} s^{-1}," J. Appl. Phys., **65** (4) 1528 (1989).

[13] M.P. Desjarlais, "Practical Improvements to the Lee-More Conductivity Near the Metal-Insulator Transition," Contrib. Plasma Phys., **41** (2-3) 267-270 (2001); M.P. Desjarlais, J.D. Kress and L.A. Collins, "Electrical conductivity for warm, dense aluminum plasmas and liquids," Phys. Rev. E, **66**, 025401(R) (2002).

[14] T. Hupf, C. Cagran, G. Lohofer, and G. Pottlacher, "Electrical resistivity of high melting metals up into the liquid phase," (V, Nb, Ta, Mo, W)," J. Phys.: Conf. Series, **98**, 062002 (2008).

[15] P.D. Desai, T.K. Chu, H.M. James, and C.Y. Ho, "Electrical Resistivity of Selected Elements," J. Phys. Chem. Ref. Data, **13** (4) 1069 (1984).

[16] M. van Thiel, "Compendium of Shock Wave Data, Section A1," Technical Report UCRL-50108, Vol. 1, Rev. 1, Lawrence Livermore Laboratory, Livermore, CA, June 1977.

[17] S.P. Marsh, "LASL Shock Hugoniot Data," University of California Press, Berkeley, CA (1980).

[18] H.J. McSkimin and P. Andreatch, Jr., "Elastic moduli of diamond as a function of pressure and temperature," J. Appl. Phys., **43** (7) 2944, (1987).

[19] J. Asay, private communication, March 2010.

[20] R. Hill, The Mathematical Theory of Plasticity, reprinted in the Oxford Classic Series, Oxford University Press, Oxford (1998).

[21] J.W. Swegle and L.C. Chhabildas, "A Technique for the Generation of Pressure-Shear Loading Using Anisotropic Crystals," in Shock Wave and High-Strain-Rate Phenomena in Metals, edited by M.A. Meyers and L.E. Murr, Plenum Press, NY, 1981, pp. 401-415.

[22] A.F. Bower, Applied Mechanics of Solids, CRC Press, Boca Raton, FL (2010).

[23] L.D. Landau and E.M. Lifshitz, Theory of Elasticity, 2nd edition, Pergamon Press, Oxford (1970).

[24] K.W. Struve, *et al*., "Comparison of the performance of the upgraded Z with circuit predictions," 17th IEEE Int. Pulsed Power Conference, F. Peterkin and R. Curry, eds., pp. 1147 (2009).